HHS Public Access

Author manuscript

Endocr Relat Cancer. Author manuscript; available in PMC 2016 August 01.

Published in final edited form as:

Endocr Relat Cancer. 2015 October ; 22(5): 777–792. doi:10.1530/ERC-14-0302.

RhoB upregulation leads to either apoptosis or cytostasis through differential target selection

Laura A. Marlow[1], **Ilah Bok**[1], **Robert C. Smallridge**[1,2,3], and **John A. Copland**[1,3,*]

[1]Department of Cancer Biology, Mayo Clinic, 4500 San Pablo Road, Jacksonville, Florida 32224

[2]Internal Medicine Department, Division of Endocrinology, Mayo Clinic, 4500 San Pablo Road, Jacksonville, Florida 32224

[3]Endocrine Malignancy Working Group, Mayo Clinic, 4500 San Pablo Road, Jacksonville, Florida 32224

Abstract

Anaplastic thyroid carcinoma is a highly aggressive undifferentiated carcinoma with a mortality rate near 100% that is due to an assortment of genomic abnormalities that impedes the success of therapeutic options. Our laboratory has previously identified that RhoB upregulation serves as a novel molecular therapeutic target and agents upregulating RhoB combined with paclitaxel lead to antitumor synergy. Knowing that histone deacetylase (HDAC) 1 transcriptionally suppresses *RhoB*, we sought to extend our findings to other HDACs and to identify the HDAC inhibitor (HDACi) that optimally synergize with paclitaxel. Here we identify HDAC6 as a newly discovered *RhoB* repressor. By using isoform selective HDAC inhibitors (HDACi) and shRNAs, we show that RhoB has divergent downstream signaling partners, which are dependent on the HDAC isoform that is inhibited. When RhoB upregulates only p21(cyclin kinase inhibitor) using a class I HDACi (romidepsin), cells undergo cytostasis. When RhoB upregulates BIM_{EL} using class II/(I) HDACi (belinostat or vorinostat), apoptosis occurs. Combinatorial synergy with paclitaxel is dependent upon RhoB and BIM_{EL} while upregulation of RhoB and only p21 blocks synergy. This bifurcated regulation of the cell cycle by RhoB is novel and silencing either p21 or BIM_{EL} turns the previously silenced pathway on, leading to phenotypic reversal. This study intimates that the combination of belinostat/vorinostat with paclitaxel may prove to be an effective therapeutic strategy via the novel observation that class II/(I) HDACi antagonize HDAC6-mediated suppression of *RhoB* and subsequent BIM_{EL}, thereby promoting antitumor synergy. These overall observations may provide a mechanistic understanding of optimal therapeutic response.

*Correspondent footnote: John A. Copland, Department of Cancer Biology, Mayo Clinic, 4500 San Pablo Road, Jacksonville, Florida, 32224, 904-953-6120 phone, 904-953-0277 Facsimile, copland.john@mayo.edu.

Declaration of interest: nothing to disclose

Author contributions: Laura Marlow contributed to experimental conception and design, acquisition of data, interpretation of data, and writing / revision of manuscript. Ilah Bok contributed to acquisition of data, interpretation of data and editing of manuscript. Robert Smallridge contributed to experimental conception and design, editing of manuscript and providing funding. John Copland contributed to experimental conception and design, editing / approval of manuscript and providing funding.

Keywords

anaplastic thyroid carcinoma; HDAC; RhoB; BIM; p21

Introduction

No effective therapy or standard of care exists for ATC patients since it is a rapidly progressing cancer with median survival of 3–5 months with near 100% fatality (Smallridge, et al. 2009). These patients desperately needed new interventional therapy to manage this malignant disease. Using genomic profiling, we previously detailed a novel signaling pathway where RhoB in combination with the microtubule stabilizer, paclitaxel, had antitumor synergy in ATC (Marlow, et al. 2009). An intriguing preclinical finding was that a novel peroxisome proliferator activated receptor gamma (PPARγ) agonist, efatutazone (a.k.a. CS-7017, RS5444), induced RhoB expression causing an upregulation of the cyclin kinase inhibitor gene (*CDKN1A*) and its $p21^{WAF1/CIP1}$ (p21) protein. p21 was necessary for inhibition of cell proliferation via G0/G1 cell cycle arrest and by silencing *PPARγ, RhoB, or p21* we showed that the growth inhibitory effects of efatutazone was nullified (Marlow et al. 2009). Thus, we identified a sequential pathway in which efatutazone→PPARγ→RhoB→p21→cell cycle arrest. In addition, we found that paclitaxel in combination with efatutazone possessed strong proapoptotic cell death synergy, doubling the apoptotic effects of paclitaxel (Marlow et al. 2009). These *in vitro* and *in vivo* preclinical discoveries led to a phase 1 clinical trial in ATC patients combining efatutazone with paclitaxel for which we have recently reported encouraging results (Smallridge, et al. 2013). A multisite national Phase 2 clinical trial was opened in September 2014.

Here we further examine the role of RhoB in ATC. RhoB is a member of the Ras superfamily of isoprenylated small GTPases which unlike oncogenic RhoA and RhoC, possesses antitumor activity (Prendergast 2001b). Depending upon its cellular localization, RhoB exerted different functions. In the cytoplasm, it regulated actin organization and vesicle transport. *RhoB* was suppressed but not mutated in numerous cancers that include head & neck, colon, and lung cancers (Adnane, et al. 2002; Agarwal, et al. 2002; Mazieres, et al. 2004). Multiple stimuli upregulated or suppressed *RhoB* including stress and growth stimuli (Ader, et al. 2002; Fritz and Kaina 2001; Ishida, et al. 2004; Jiang, et al. 2003; Jiang, et al. 2004). Multiple therapeutics have been discovered to upregulate RhoB and were associated with antitumor activity; these include farnesyl transferase inhibitors, HDAC inhibitors (HDACi), hydroxymethylglutaryl-CoA reductase inhibitor (statins), and glucocorticoids (Agarwal et al. 2002; Allal, et al. 2002; Chen, et al. 2006; Furumai, et al. 2002; Marlow, et al. 2010; Prendergast 2001a).

RhoB activity has been shown to cause apoptosis in transformed cells (Prendergast 2001b). However, we found that efatutazone induced RhoB mediated cell cycle arrest and not apoptosis (Copland, et al. 2006; Marlow et al. 2009). To seek a more powerful therapeutic than efatutazone plus paclitaxel and to better understand RhoB mechanism(s) of action, we reasoned to use HDACi plus paclitaxel, since previous studies showed that the use of a class I/II HDACi led to apoptosis (Borbone, et al. 2010; Catalano, et al. 2007; Chan, et al. 2013;

Mitsiades, et al. 2005). Additionally, histone deacetylase 1 (HDAC1) can directly suppress *RhoB* mRNA via binding to an inverted CCAAT box in the *RhoB* promoter (Wang, et al. 2003). We hypothesized that by re-expressing RhoB, HDACi leads to apoptosis and antitumor synergy when combined with paclitaxel for improved patient prognosis.

HDACi modulate acetylation by targeting histone deacetylases and serve as powerful antitumor agents since they induce differentiation and apoptosis via transcriptional modulation. To date, a Class I HDACi, romidepsin (depsipeptide / FK228) and a Class II/(I) HDACi, vorinostat (SAHA / MK-0683), were FDA approved for treating cutaneous T-cell lymphoma (Nebbioso, et al. 2009; New, et al. 2012; Prince, et al. 2009). Another class II/(I) HDACi, belinostat (PXD101) was FDA approved for relapsed or refractory peripheral T-cell lymphoma (Lee, et al. 2015) and panobinostat (LBH589) was recently approved for multiple myeloma (2015). Other HDACi are currently in phase II clinical trials including: givinostat (ITF2357), mocetinostat (MGCD0103), quisinostat (JNJ-26481585), pracinostat (SB939), resminostat (4SC-201), entinostat (MS-275), abrexinostat (PCI-24781), and valproic acid as a HDACi (previously FDA approved for epilepsy). Class I HDACs encompassed HDAC1-3 and 8 while Class II, included HDAC4-7, 9 and 10 (Bertos, et al. 2001; Zhou, et al. 2001). Class III, also known as the Sir2 (silent information regulator 2) family, consisted of seven genes related to yeast Sir2, and possess nicotinamide-adenine dinucleotide (NAD+)-dependent deacetylase activity (Vaziri, et al. 2001). Class IV have characteristics of both class I and class II HDACs with HDAC11 being its only member (Gao, et al. 2002).

Our current investigation used clinically relevant HDACi to delineate RhoB-mediated signaling pathways which bifurcate depending upon the class of HDACi used. When a class I HDACi led only to p21 upregulation and G0/G1 cell cycle arrest, then no synergy with a cytotoxic agent occurred. The upregulation of BIM_{EL} and G2/M arrest in ATC cell lines led to induction of apoptosis and antitumor synergy with cytotoxic therapy. For the first time, we described that HDAC6 transcriptionally suppressed *RhoB* to mediate the pro-apoptotic effects of class II/(I) HDACi. Both HDAC1 and HDAC6 upregulated *RhoB*, *CDKN1A* and *BIM* mRNA and thus, the absence of p21 or BIM protein expression after HDACi treatment was regulated via proteosome protein degradation mechanisms. We further demonstrated that HDAC1 and HDAC6 protein levels were elevated in ATC patient tissues indicative of potential therapeutic relevance.

Materials and Methods

Reagents

The HDACi, belinostat (PXD101) and vorinostat (SAHA / MK-0683) and romidepsin (depsipeptide / FK-228) were purchased from Selleck (Houston, TX). Paclitaxel, MG132 and DMSO solvent were purchased from Sigma-Aldrich (St. Louis, MO).

Cell culture

THJ-11T (*KRAS*, *TP53*, *TERT*), THJ-16T (*PI3KCA*, *TP53*, *TERT*), THJ-21T (*BRAF*, *TP53*, *TERT)* and THJ-29T (*APC*, *TP53*, *TERT*) ATC cell lines were originated in our laboratory (Marlow et al. 2010) and were short-tandem repeat (STR) verified and validated to the

respective patient's ATC tissue. The *APC* mutation for THJ-29T was identified by Drs. James Fagin and Jeffrey Knauf as well as validating the other mutations (personal communication). Thyroid cells were maintained in RPMI 1640 medium (Cellgro, Manassas, VA) supplemented with 5% fetal bovine serum (Hyclone, Logan, UT), non–essential amino acids (Cellgro), sodium pyruvate (Cellgro), HEPES (Cellgro) and penicillin-streptomycin-amphotericin B (Cellgro) at 37°C in a humidified atmosphere with 5% CO_2. 293FT cells were purchased from (Invitrogen, Carlsbad, CA) and were maintained in DMEM as per the manufacturer's protocol along with 500 μg/ml neomycin (MP Biomedical, Solon, OH).

Luciferase Reporter Gene Analysis

Cells were plated in 12-well culture plates (Genesee Scientific, San Diego, CA) at 1×10^5 cells/well. Once adhered, cells were transiently transfected using Lipofectamine 2000 (Invitrogen) with 25 ng pRL-CMV-renilla (Promega, Madison, WI) and 1 μg pGL2/p21-luc 2280bp (provided by Dr. Rebecca Chinery), or pGL3/RhoB-luc 1876bp (provided by Daniel Tovar, Institut Claudis Regaud, Toulouse, France) along with 0.5 μg each of MISSION shRNA pLKO.1 constructs HDAC1 through HDAC11 (Sigma-Aldrich). After 24 hours, cells were lysed using Promega's Dual Luciferase assay kit per the manufacturer's protocol. Luciferase activity was measured using a Veritas luminometer (Promega) and the enzyme activity was normalized for transfection efficiency based upon renilla activity levels and reported as relative luminescent units ± S.D. Comparisons were analyzed by two-tailed paired Student's *t*-test. $p < 0.05$ was considered statistically significant.

Lentivirus and infections

Self-inactivating shRNA lentiviruses were generated using MISSION shRNA pLKO.1 constructs that included a nontarget control which was a random scrambled sequence (SHC002), *RhoB* 839 (clone NM_004040.2-839s1c1) was previously validated (Vishnu, et al. 2012), *p21* 562 (clone NM_000389.2-562s1c1), *BIM* 537 and 541 (BCL2L11) (clones NM_138621.x-537s1c1, NM_138621.x-541s1c1), *HDAC1* (NM_004964.2-789s1c1), *HDAC6* 3384 and 3840 (NM_006044.2-3384s1c1, NM_006044.2-3840s1c1) (Sigma-Aldrich). Lentiviruses were packaged using 293FT cells via transfection of the pLKO.1 constructs along with packaging plasmids using OptiMEM and Lipofectamine 2000 (Invitrogen). The packaging plasmids were originally made by Didier Trono supplied by Addgene (Cambridge, MA), which included: pMDLg/pRRE (gag/pol) (plasmid #12251), pRSV-Rev (plasmid #12253), and pMD2.G (VSVG) (plasmid #12259). Supernatants were collected 72 h post-transfection, passed through a 0.45 μm PVDF syringe filter (Millipore, Bedford, MA) and applied to cells for infection along with 5 μg/ml polybrene (American Bioanalytical, Natick, MA). Cells were selected with puromycin (Fisher Scientific, Pittsburgh, PA).

Proliferation assays

For dose out curves and lentiviral infected clones, cells were treated with belinostat, vorinostat, romidepsin or paclitaxel at the indicated doses and were counted on a Coulter Particle Counter (Beckman, Brea, CA). When applicable, IC_{50} was determined via extrapolation of 50% growth on log scale to the corresponding drug concentration. Using the

ratio of the IC_{50}, the proportion of each compound needed in a combination dose was calculated. Experiments were then carried out using HDACi, paclitaxel and a fixed ratio combination of both at the indicated doses in clear-bottom black plates (Costar, Corning, NY) and analyzed using the CyQUANT proliferation assay kit (Invitrogen) as per manufacturer's protocol for relative fluorescence units. Drug interactions were analyzed using CalcuSyn® (Biosoft, Cambridge, UK). Determination of synergy, additivity or antagonism was based on the multiple drug effect equation of Chou and Talalay and was quantified by the combination index (CI). CI = 1 indicates an additive effect, < 1 is synergy and > 1 is antagonism (Chou and Talalay 1984).

Flow cytometry

Cells were grown to ~ 50% confluence prior to treatment. Floating cells were collected from the media and adhered cells were collected using Accutase (Innovative Cell Technologies, San Diego, CA). For cell death analysis, cells were washed with cold PBS and resuspended in FACS binding buffer (PBS, 1% bovine serum albumin fraction V, 25 mM HEPES, 1 mM EDTA) followed by staining with propidium iodide (BD Pharmingen, San Jose, CA). Annexin V was not used since the cells were strongly adherent. For cell cycle analysis, cells were resuspended in cold 0.5% glucose/PBS and fixed in 70% ethanol. For staining with propidium iodide, cells were resuspended in 0.1% triton X-100/PBS along with RNase A (Sigma-Aldrich). FACS analysis was performed on Accuri C6 flow cytometer (Accuri, Ann Arbor, MI) using 100,000 events. Unstained cells were used as controls for setting the population parameters and overlay of histograms shows no deviation or drift of channels. More than a 5% change from the control was considered statistically significant. For cell cycle statistics, data was analyzed using MultiCycle AV (Phoenix Flow Systems, San Diego, CA) with FCS Express plug-in (De Novo, Los Angeles, CA).

RNA isolation and quantitative PCR (QPCR)

Total mRNA was isolated from cells using Purelink RNA isolation kit (Invitrogen) with DNase treatment per the manufacturer's protocol and the O.D. 260/280 ratio of the mRNA was at least 1.8. Two-step quantitative reverse transcriptase-mediated real-time PCR (QPCR) was used to measure changes in mRNA levels. The RT step was achieved by synthesizing cDNA using the High Capacity Reverse Transcription kit as per the manufacturer's protocol (Applied Biosystems Foster City, CA). The PCR step was done using TaqMan® Fast Universal PCR Master Mix (Applied Biosystems) and TaqMan® FAM™ dye-labeled probes for *RhoB*(Hs00269660_s1), *p21*(Hs00355782_ml), *BIM*(BCL2L11, Hs00375807_ml), HDAC1(Hs00606262_g1), HDAC2(Hs00231032_m1), HDAC3(Hs00187320_m1), HDAC4(Hs01041648_m1), HDAC5(Hs00608366_m1), HDAC6(Hs00195869_m1), HDAC7(Hs00248789_m1), HDAC8(Hs00954353_g1), HDAC9(Hs00206843_m1), HDAC10(Hs00368899_m1), HDAC11(Hs00978041_m1), and *POLR2A* (Hs00172187_ml). Data was normalized to POLR2A for each sample. Fold change values between nontargets and shRNA samples were calculated using the ΔΔCt method (Schmittgen and Livak 2008).

Cell lysis and western blot analysis

Cells were grown to ~ 50% confluence prior to treatment. Floating and adhered cells were collected via scraping and lysed in M-PER extraction buffer (Pierce, Rockford, IL) containing protease inhibitor cocktail (Roche, Mannheim, Germany) and phosphatase inhibitor (Pierce, Rockford, IL). Protein concentrations were measured by bicinchoninic acid (BCA) assay (Pierce) and 30 μg were loaded on 4–12% Bis-Tris/MES gels (Invitrogen) and then transferred to 0.2 μm Immobilon-P membranes (Millipore). The membranes were hybridized overnight at 4 °C with the following antibodies: BIM, PARP, Acetyl H3 L9 (Cell Signaling, Danvers, MA); α-tubulin, acetyl a-tubulin, β-actin (Sigma-Aldrich); RhoB, p21, HDAC1, HDAC6 (Santa Cruz Biotechnology, Santa Cruz, CA). Secondary species-specific horseradish peroxidase-labeled antibodies were from Jackson Immunoresearch (West Grove, PA). Detection was performed using Supersignal chemiluminescence kit (Pierce). Protein expression from Western blot analysis was quantitated using Image Quant 5.0 (Molecular Dynamics, GE Healthcare, Piscataway, NJ). Blots were background corrected and normalized to loading controls.

Immunohistochemistry (IHC)

A tissue microarray (TMA) was made from archival formalin fixed paraffin embedded samples under Mayo Clinic IRB approval. TMA tissues were cut into 5 mm sections, deparaffinized, hydrated, antigen retrieved and blocked with Diluent that contained Background Reducing Components (Dakocytomation, Denmark). Immunostaining was done with HDAC1 at 1:100 (Santa Cruz) and HDAC6 at 1:100 (Cell Signaling). The Envision Dual Labeled Polymer kit (DAKOCytomation) was used according to the manufacturer's instructions and then lightly counterstained with Gill I hematoxylin (Sigma-Aldrich) before dehydration and mounting. Images were obtained at 20X using Scanscope XT (Aperio Technologies, Vista, CA) and the staining of the TMA punches were scored using an algorithm in the Imagescope software (Aperio Technologies) created by a histologist based upon signal intensity (0, 1+, 2+, 3+). H score was then calculated based upon signal intensity and percentage: H= (1+%*1)(2+%*2)(3+%*3). Cases were excluded from the study if a section could not be assigned a score due to insufficient quantity of tumor tissue present.

Results

Downstream pathway differences of class I and II histone deacetylase (HDAC) inhibitors (HDACi)

Belinostat and vorinostat were hydroxamate class II/(I) (stronger class II than class I) HDACi while romidepsin was a cyclic peptide class I HDACi. Dose response curves for cell proliferation using 4 ATC cell lines were performed with belinostat (PXD101), vorinostat (SAHA) or romidepsin (FK-228) ranging from 0.1 nM to 1 μM for determination of IC_{50} (50% inhibitory concentration). The class II/(I) inhibitors (Khan, et al. 2008; Mai, et al. 2005) belinostat yielded an IC_{50} of 400 nM for both THJ-16T and THJ-21T and 250 nM for both THJ-29T and THJ-11T while vorinostat yielded an IC_{50} of 250 nM for both THJ-16T and THJ-29T and 450 nM for THJ-11T and 500 nM for THJ-21T (Figure 1A, **panels 1–2**). The class I inhibitor (Furumai et al. 2002), romidepsin yielded an IC_{50} of 0.4 nM (Figure

1A, **panel 3**) for each of the cell lines. Cell death effects of these HDACi were examined by flow cytometry and cell death was seen with belinostat and vorinostat treatments in all cell lines while romidepsin had no effect upon cell death in THJ-16T and THJ-29T. Belinostat induced cell death by 18 to 34% and vorinostat induced cell death by 10 to 19%. Romidepsin only induced cell death in THJ-11T and THJ-21T by ~10% (Figure 1B). For both class II/(I) HDACi, THJ-29T exhibited greater sensitivity and the class I HDACi had no cell death effect. It should be noted that THJ-16T was *PI3KCA, TP53, Rb* mutant, THJ-11T was *KRAS* mutant, THJ-21T was *BRAF,TP53, Rb* mutant and THJ-29T was *Rb* mutant which may have influenced responses to each of the HDACi (Marlow et al. 2010).

Apoptosis was examined via PARP cleavage. Belinostat and vorinostat treatments induced cleaved PARP in all 4 ATC cell lines while romidepsin treatment did not in THJ-16T and THJ-29T (Figure 1C). Previous publications demonstrated that vorinostat induced apoptosis via upregulation of the proapoptotic Bcl2-interacting mediator of cell death, BIM, which triggered cytochrome c release from the mitochondria leading to apoptosis (Zhao, et al. 2005). We found that the BIM isoform, BIM_{EL} (extended length) (Ramesh, et al. 2009) was strongly induced by Class II/(I) HDACi, belinostat, and vorinostat in all 4 cell lines, and weakly with Class I HDACi romidepsin in THJ-11T and THJ-21T (Figure 1C) with no change in XIAP, survivin, Bax, p-Bcl2 (data not shown). Based upon previous studies of romidepsin's effects in ATC cells and that RhoB and p21 are repressed by HDAC1, they were also examined by western blot (Marlow et al. 2010; Marlow et al. 2009; Sambucetti, et al. 1999; Wang et al. 2003). All three HDACi induced RhoB protein expression while p21 expression was dependent upon the HDACi and cell line. Romidepsin induced p21 in all 4 cell lines while belinostat induced p21 in THJ-21T and vorinostat induced p21 in THJ-11T and THJ-21T. Since BIM degradation can be regulated by Erk signaling (Akiyama, et al. 2009; Chakraborty, et al. 2013), p-Erk and p-Akt (data not shown) expression was examined and no consistent change in expression was found within or across the four ATC cell lines examined (Figure 1C).

To test if THJ-16T and THJ-29T functioned differently at the transcriptional level, *RhoB* and *p21* reporter activity were examined. All three HDACi induced *RhoB* (~7–27 fold) and *p21* (~4–9 fold) transcription (Figure s1). Endogenous *RhoB* (~4–7 fold, panel 1) and *p21* (~7–18 fold, panel 2) mRNA levels were also induced by all three HDACi in all 4 cell lines (Figure 2A, **panels 1–2**). *BCL2L11 (BIM)* mRNA was also measured with an induction of ~2–6 fold with greater effects seen with belinostat and vorinostat in all 4 cell lines (Figure 2A, **panel 3**). Thus, in order to address the inconsistencies in mRNA levels and protein expression, protein stability was assessed using a time course with or without the proteasome inhibitor, MG132 using THJ-16T and THJ-11T as a representative. As expected, RhoB expression was consistently upregulated by 6h in both cell lines for all 3 HDACi (Figures 2B, C, and D). Interestingly, p21 protein in THJ-16T was greatly induced by belinostat at 12h and completely degraded by 24h, which could be rescued by the proteosome inhibitor, MG132. In THJ-11T, p21 protein levels remained consistent over the time course. BIM_{EL} protein levels were upregulated by belinostat as early as 6h and BIM_{EL} protein was not targeted for proteosome degradation (Figure 2B). Vorinostat had not induced p21 protein in THJ-16T at any time point indicating rapid degradation except when

MG132 rescued p21 at 24h while p21 remained upregulated as early as 6h in THJ-11T. By 24h in THJ16T, vorinostat upregulated BIM_{EL} protein levels and it was not targeted for proteosome degradation. However, in THJ-11T, BIM_{EL} protein levels were increased by 6h and at 12h it was further enhanced with MG132, which indicated some proteasome degradation, but this did not occur at 24h (Figure 2C). With romidepsin in THJ-16T, p21 protein was induced by 6h and remained elevated regardless of proteosome inhibition by MG132 while BIM_{EL} protein was not seen until 24h with MG132, which indicated rapid degradation. Interestingly, p21 was not elevated until 24h in THJ-11T while BIM_{EL} protein levels were seen as early as 6h with no effects seen with MG132 (Figure 2D). Thus, if degraded, both p21 and BIM_{EL} protein can be rescued by MG132.

In order to demonstrate that the HDACi were RhoB-dependent, *RhoB* was silenced using *RhoB 839* shRNA; specificity of this shRNA against RhoB has been previously demonstrated (Marlow et al. 2010; Marlow et al. 2009; Vishnu et al. 2012). The level of *RhoB* silencing in these models ranged from 35 to 65% as examined by QPCR (Figure s2A). When *RhoB* was silenced during HDACi treatment, proliferative inhibition was reversed by ~40–100% (Figure 3A). Using THJ-16T and THJ-21T as representative, western blots confirmed that RhoB was silenced by *RhoB* shRNA and that p21 induced by romidepsin was blocked when upstream *RhoB* was silenced. Induced BIM_{EL} was also blocked with *RhoB* silencing (Figure 3B). Therefore, upregulation of *RhoB* was necessary for p21 and BIM_{EL} expression.

Combinatorial therapy with HDACi and paclitaxel

An assortment of findings which included, RhoB-dependent antitumor synergy with paclitaxel and a PPARγ agonist (Marlow et al. 2009), paclitaxel stabilizing BIM_{EL} expression in breast cancer models (Akiyama et al. 2009), and having some efficacy in patients with ATC (Ain, et al. 2000) inspired us to combine paclitaxel with the three HDACi used in this study. We tested each HDACi in combination with paclitaxel for antitumor synergy with the expectation of observing RhoB-dependent antitumor synergy. The concentration at which 50% inhibition of cell proliferation (IC50) for paclitaxel was determined and yielded an IC_{50} of 0.5 nM for THJ-16T, 2 nM for THJ-29T and 4 nM for THJ-11T and THJ-21T (Figure s3). Synergy between each HDACi and paclitaxel was assessed using the median effects model of Chou-Talalay (Chou and Talalay 1984). Belinostat combined with paclitaxel yielded synergy in THJ-16T (CI_{ED50}=0.12), THJ-29T (CI_{ED50}=0.47), THJ-11T (CI_{ED50}= 0.89) and THJ-21T (CI_{ED50}= 0.47) as shown by the left shifts of the dose curves (Figure 4A). Vorinostat combined with paclitaxel also yielded synergy with CI_{ED50}=0.49, CI_{ED50}=0.36, CI_{ED50}= 0.62 and CI_{ED50}= 0.31, respectively (Figure 4B). However, combinatorial romidepsin and paclitaxel demonstrated no synergy and no left shift (CI_{ED50}=1.1, CI_{ED50}=1.4) in THJ-16T and THJ-29T while synergy was observed in THJ-11T (CI_{ED50}= 0.63) and THJ-21T (CI_{ED50}=0.52) (Figure 4C). Combinatorial index (CI) values of less than 1 are considered synergistic. Cell death analysis with combinatorial therapy demonstrated similar results with enhanced cell death with the Class II/(I) HDACi combined with paclitaxel in all 4 cell lines (Δ15–40%), but not with romidepsin in THJ-16T and THJ-29T where BIM_{EL} was not elevated. Enhanced cell death with romidepsin and paclitaxel was seen in THJ-11T (Δ18%) and THJ-21T (Δ18%)

(Figure 4D). Thus, in HDACi treated cells where BIM_{EL} was elevated, apoptosis and combinatorial therapy antitumor synergy occured regardless of p21 expression levels.

The combinatorial effect with belinostat could be reversed when *RhoB* was silenced in representative THJ-16T cells (CI_{ED50}=1.1) with the loss of a leftward curve shift (Figure 5A). As well, the combinatorial effect with vorinostat could be reversed when RhoB was silenced in THJ-16T (CI_{ED50}=1.1) also (Figure 5B). A previous publication using valproic acid (class I/II HDACi) in ATC cells indicated that paclitaxel via microtubule stabilization promoted acetylated α-tubulin as the mechanism of synergy (Catalano et al. 2007). We thus examined belinostat or vorinostat in combination with paclitaxel for this potential explanation of synergy. However, there was no consistent enhancement of acetyl α-tubulin in the presence of paclitaxel in either of the 4 cell lines (Figure 5C). Thus, our results indicated that loss of combinatorial synergy was dependent upon RhoB signaling and not acetyl α-tubulin.

Flipping the RhoB→p21 and RhoB→BIM_{EL} pathway switch

To identify the role of p21 upregulation in romidepsin treated cells, p21 was silenced. p21 shRNA constructs were screened by QPCR and *p21 clone 562* was identified to effectively silence *p21* mRNA (~65%) (Figure s2B). Western blot analysis using the *p21 562* construct in THJ-16T cells showed that romidepsin treatment induced RhoB, but when *p21* was silenced, BIM_{EL} and PARP cleavage were induced (Figure 6A). Cell cycle analysis showed that romidepsin treatment shifted nontarget control cells to G1 phase (~Δ15.7%). However, when *p21* was silenced with romidepsin, G2 phase was increased by ~Δ10% with a sub-G0 population to the left of the histogram (Figure 6B). Cell death analysis by flow cytometry in THJ-16T showed that when *p21* was silenced, cell death was evoked in romidepsin treated cells by Δ12% and that combinatorial cell death effects enhanced by ~10% with an overall cell death of 30% (Figure 6C). Combinatorial effects were then examined via cell proliferation and romidepsin with paclitaxel showing synergy (CI_{ED50}=0.24) when *p21* was silenced (Figure 6D). Thus, silenced p21 allowed BIM_{EL} to be expressed at the protein level reversing the phenotype to re-establish synergy.

We next tested whether silencing BIM_{EL} would lead to loss of synergy. BIM_{EL} shRNA constructs were screened by QPCR and BIM_{EL} *clones 537* and *541* were identified to effectively silence *BIM* mRNA by ~40% and ~50%, respectively (Figure s2C). Western blot analysis of THJ-16T using BIM_{EL} *541* construct showed belinostat/vorinostat treatments still induced RhoB, but when BIM_{EL} was silenced, PARP cleavage was lost. In the presence of *BIM* shRNA, BIM_{EL} was silenced and p21 protein expression was induced in the presence of both belinostat and vorinostat treatments (Figure 7A). Cell cycle analysis showed that belinostat and vorinostat increased the percent of cells in G2 phase by ~Δ19% and induced a sub-G0 subpopulation versus that of nontarget control cells. However, when BIM_{EL} was silenced in treated cells, the G1 phase was shifted by ~Δ17.7 and Δ15.7% with diminished sub-G0 populations, respectively (Figure 7B). Furthermore, in belinostat and paclitaxel treated THJ-16T cells with BIM_{EL} silenced, synergy was lost (CI_{ED50}=1.1) (Figure 7C). Thus, combinatorial synergy can be reversed by silenced BIM_{EL} presumably via re-expression of p21 protein leading to cytostasis.

HDAC1 and HDAC6 are repressors of RhoB

Since there were differential HDACi effects on *RhoB* signaling leading to p21 or BIM_{EL}, all HDACs were examined from class I, II and IV. Using multiple shRNA constructs against *HDAC1 to 11*, THJ-16T cells were transiently transfected and the level of silencing was examined by QPCR for the corresponding HDAC (Figure 8A). Luciferase reporter assay of the *RhoB* promoter co-transfected with each of the verified HDAC shRNAs were used to screen transcriptional regulation for HDAC 1 – 11.s. Activation of the *RhoB* promoter was observed when *HDAC1* was silenced by *clone 789* and *HDAC6 clones 3384 and 3840* (Figure 8B). For verification, THJ-29T was tested using positive and negative constructs from the panel. Again, *HDAC1 789*, *HDAC6 3384* and *3840* showed RhoB promoter activity while the non-effective HDAC shRNAs did not (Figure s4). Thus, both HDAC1 and HDAC6 repressed the *RhoB* promoter and to our knowledge, this is the first report of *RhoB* repression by HDAC6. For clinical relevance, IHC was performed on patient normal and ATC tissues. Both HDAC6 (H = 125.8, n=59) and HDAC1 (H=184.2, n=52) were overexpressed in ATC as compared to normal tissues (H=64.1 (n=35), H=129.0 (n=23), respectively), which indicated that HDAC6 and HDAC1 may be viable molecular therapeutic targets (Figure 8C).

Direct targeting of *HDAC1* or *HDAC6* via shRNA was used to mimic the HDACi to further verify transcriptional suppression of RhoB, BIM_{EL} and p21. Using the *HDAC1 789* and *HDAC6 3384* clones in THJ-16T, QPCR revealed that *RhoB, p21* and *BIM* mRNA were all induced when *HDAC1* or *HDAC6* were silenced (Figure 9A). For protein expression, silenced *HDAC1* or *HDAC6* led to RhoB induction in all 4 cell lines. Unique to THJ-16T and THJ-29T cells, silenced *HDAC1* led to p21 induction only while silenced *HDAC6* led to BIM_{EL} induction only. On the other hand, silenced HDAC1 or HDAC6 induced both p21 and BIM_{EL} in *KRAS* mutant THJ-11T and *BRAF* mutant THJ-21T cells (Figure 9B). These 4 cell lines were also growth inhibited by ~45–65% by *HDAC1* or *HDAC6* shRNAs (Figure 9C). Flow cytometry of the shRNA clones showed that cell death was induced by ~10–18% with *HDAC6* silenced in the 4 cell lines. However, no cell death was detected upon silenced *HDAC1* in THJ-16T and THJ-29T, which had p21 but no BIM_{EL} expression. Conversely, cell death was detected upon silenced *HDAC1* in THJ-11T (7%) and THJ-21T (6%) where both p21 and BIM_{EL} expression were elevated (Figure 9D). Overall, the HDAC shRNA data corroborated the effects seen with belinostat, vorinostat, and romidepsin.

Discussion

In this study, cell proliferation was inhibited using both class I and class II(I) HDAC inhibitors in a dose responsive fashion in four recently developed patient derived ATC cell lines harboring different driver mutations (*BRAF, PI3KCA, KRAS, APC).* Clear distinctions between cell lines in response to the different HDACi arose related to cell cycle regulation (G0/G1 vs G2/M) dictating cytostasis or cell death, mediators of cell cycle regulation (p21 vs BIM_{EL}), and response to combinatorial therapeutic (synergy vs no synergy). These findings were dependent on whether upregulated RhoB was followed by either p21 exclusively or BIM_{EL} with/without p21; this differential protein expression was regulated in part by the proteosome since both *BIM* and *CDKN1* mRNA were upregulated by both class I

and II/I HDACi. In generalizing the results, G2/M arrest, apoptotic cell death and paclitaxel combinatorial synergy resulted with upregulated BIM_{EL} protein regardless of p21 protein status. This occurred in response to class II/I HDACi in all cell lines and class I HDACi in THJ11T and THJ-21T but not THJ-16T and THJ29T. Conversely, when romidepsin, the class I HDACi, induced only p21 protein (THJ-16T and THJ-29T), G0/G1 cell cycle arrest with cytostasis occurred and p21 was responsible for lack of synergy with combined paclitaxel therapy. These findings were summarized in our models as shown in Figure 10.

In the past, we and others have observed RhoB-mediated induction of p21 (Du and Prendergast 1999; Marlow et al. 2009) or BIM_{EL} (Srougi and Burridge 2011). Alternatively, HDACs directly suppressed *p21* and *BIM_{EL}* transcription by binding to their respective promoters (Chan et al. 2013; Mazieres, et al. 2005; Wang, et al. 2004; Zhao et al. 2005). Belinostat and vorinostat have been shown to induce *p21* transcription and translation that was p53-dependent in thyroid cancer cells via the zinc transcription factor, Sp1 (Chan et al. 2013; Mitsiades et al. 2005; Wang et al. 2004). In our models, p21 expression was induced by these agents in both p53 wild-type (THJ-11T, THJ-29T) and p53 mutant (THJ-16T, THJ-21T) cells. Furthermore, vorinostat had been shown in other cancer models to recruit E2F1 to the *BIM* promoter for inducing BIM_{EL} expression (Zhao et al. 2005). Our current study demonstrated both HDACi and RhoB-dependent transcriptional induction of *p21* and *BIM_{EL}* mRNA, whereby RhoB transcription was also HDACi-dependent (HDACi→ RhoB→ p21 and/or BIM_{EL}).

Moreover, transcription of the *RhoB* promoter can be activated by farnesyltransferase and geranylgeranyl transferase inhibitors via HDAC1 dissociation (Delarue, et al. 2007). HDAC1 repressed *RhoB* by binding to an inverted CCAAT box in the *RhoB* promoter and its regulation was independent of Sp1 (unlike p21) (Delarue et al. 2007; Wang et al. 2003; Wang et al. 2004). In our study, we also saw HDAC1 repression of *RhoB* and to our knowledge; this was the first report of *RhoB* repression by HDAC6. However, it had been reported that with trapoxin A (pan-HDACi) treatment in lung and breast tumor cell lines, HDAC6 had no association on the *RhoB* promoter (Wang et al. 2004).

For clinical relevance, we demonstrated that HDAC6 and HDAC1 were elevated in ATC versus normal thyroid tissue. Unlike HDAC1, which resided in the nucleus, HDAC6 remained predominantly in the cytoplasm associated with microtubules and the cytoskeleton (Boyault, et al. 2007; Kaliszczak, et al. 2013; Li, et al. 2008). The mechanism by which HDAC6 inhibition led to upregulation of RhoB transcription is yet to be identified. It had been reported that transcriptional regulation of RhoB in response to UV irradiation and farnesyltransferase inhibitors (FTIs) was associated with the recruitment of the transcriptional nuclear factors NF-Y and c-Jun, and histone acetyltransferase p300 to the CCAAT or inverted CCAAT box in the proximal RhoB promoter (Ahn, et al. 2011; Kim, et al. 2014). We hypothesized that a direct cross-talk between HDAC6 and p300 (opposing enzymatic activities) could be a mechanism to regulate RhoB gene transcription upon HDAC6 inhibition. HDAC6 predominantly deacetylates non-histone proteins, including α-tubulin; p300 acetylation of HDAC6 results in decrease of HDAC6 deacetylase activity thereby tubulin deacetylation and suppression of Sp1 transcriptional activity. Thus, p300 may regulate the activity of Sp1 indirectly through HDAC6 in addition to its direct

modification of Sp1 (Ahn et al. 2011). With HDAC6 suppression, this RhoB transcriptional complex may become re-engaged. In summary, we had uncovered novel regulation of RhoB by HDAC6 and HDAC1 which then modulated another novel switch co-regulating p21 and BIM_{EL}.

Interestingly, HDAC6 is the only member, within the histone deacetylase family, that harbored a full duplication of its deacetylase homology region followed by a specific ubiquitin-binding domain at the C-terminus (Boyault et al. 2007; Li, et al. 2013). High-affinity binding of HDAC6 to ubiquitin was shown to hinder the recognition of ubiqutinated proteins by other ubiquitin-binding factors and to delay their processing by the ubiquitin proteosomal subunit (Boyault, et al. 2006). Therefore, HDAC6 blocked proteosome degradation. Others have reported that p21 and BIM_{EL} were degraded via proteosomal degradation (Akiyama et al. 2009; Altmann, et al. 2012), which may explain the absence of p21 protein in the class II(I) HDACi treated cells. In addition, *BIM* transcription was regulated by FoxO3a and RUNX3 and its degradation was regulated by Erk signaling (Akiyama et al. 2009; Chakraborty et al. 2013) and that alterations in their activities may be HDACi-specific. BIM_{EL} contained two ubiquitination sites and three ERK phosphorylation sites and belinostat had been shown to inhibit p-Akt and pErk signaling (Chan et al. 2013). Phosphorylation by p-Erk targeted BIM_{EL} for ubiquitination and proteosomal degradation (Akiyama et al. 2009). Hence, decreased pERK will stabilize BIM_{EL} expression when HDAC6 was dissociated. One study had shown that the use of Mek inhibitors in combination with romidepsin stabilized BIM_{EL} to promote apoptosis (Chakraborty et al. 2013). For romidepsin treated THJ-16T and THJ-29T cells, we showed that pErk was present and not blocked which may have led to BIM_{EL} degradation. Thus, divergent patterns of p21 and BIM_{EL} regulation were identified related to the class of HDACi used leading to differential proteosome activation.

This study documented the novel phenomenon whereby silencing of p21 or BIM_{EL} allow the other protein to be expressed thereby switching the activity of the two HDACi classes with RhoB being necessary for either cell fate to occur. The mechanism by which multifaceted RhoB differentially “decided” to promote either the p21 (cytostasis) or BIM_{EL} (apoptosis) pathway between class I and II HDACi remains to be elucidated. For example, when p21 was exclusively present, it led to G1 arrest and repression of BIM_{EL} (Collins, et al. 2005). With class II inhibitors, BIM_{EL} protein was expressed across all four cell lines regardless of cell line mutation suggesting that the mutation does not regulate proteosome activity. Silenced *p21* in romidepsin treated cells mimiced the “pro-p21” degradation activity of class II inhibitors, thus allowing BIM_{EL} expression. While intriguing, it remained to be explained why BIM_{EL} repression allowed stabilization of p21 and vice versa, why p21 repression allowed BIM_{EL} stabilization.

Interestingly, combinatorial synergy of class II/(I) HDACi was not dependent upon microtubule stabilization when combined with paclitaxel as previously reported (Catalano et al. 2007). Instead, our data indicated that activation of the BIM_{EL} pathway dictated synergy. Thus, inhibiting HDAC6 led to RhoB-mediated induction of BIM_{EL} which led to G2/M arrest and apoptosis. On the other hand, inhibiting HDAC1 led to RhoB-mediated induction of p21 which led to G1 cell cycle arrest. These divergent RhoB pathways can be flipped

between the two dictated by BIM_{EL} and p21 protein expression. Therefore, p21 and BIM_{EL} not only dictated apoptosis versus cell cycle arrest, but also dictated combinatorial synergy. This is clinically relevant since targeting BIM_{EL} for combination therapy would be most beneficial in patients with ATC. Ionizing radiation (IR) or other DNA damaging agents had been previously shown to lead to the induction of BIM_{EL} in a RhoB-dependent manner (Srougi and Burridge 2011). Therefore, we and others believed therapies should revolve around inducing expression of BIM_{EL} in cancer (Akiyama et al. 2009).

The expression of BIM_{EL} mediated by upregulated RhoB in response to therapy may be a biomarker of antitumor synergy with cytotoxic therapy such as paclitaxel. With the advent of novel specific HDAC6 inhibitors, HDAC6 may be a preferred molecular target for combinatorial therapeutic antitumor synergy, as suggested by others [reviewed in (Li et al. 2013)], especially in patients with ATC. To support this premise, belinostat had demonstrated *in vivo* antitumor activity against ATC tumors grown in athymic nude mice (Chan et al. 2013). As well, there was a single case report of successful treatment of ATC with a combination of oral valproic acid, chemotherapy consisting of cisplatin and doxorubicin, external and intra-operative radiation and surgery (Noguchi, et al. 2009). In summary, this report was the first to describe regulation of RhoB by HDAC6 and that RhoB down-stream effectors differentially regulated cell fate and chemotherapeutic synergy. These discovered differences may provide therapeutic benefit.

Supplementary Material

Refer to Web version on PubMed Central for supplementary material.

Acknowledgments

Funding: This work was supported by the National Institute of Health and Medical Research (R01CA136665; JAC, RCS), the Florida Department of Health Bankhead-Coley Cancer Research Program (FL09B202; JAC, RCS), a generous gift from Alfred D. and Audrey M. Petersen (RCS), the Francis and Miranda Childress Foundation Fund for Cancer Research (JAC), John A. and Bette B. Klacsmann Fund for Cancer Research at Mayo Clinic in Florida (JAC), and the Betty G. Castigliano Fund in Cancer Research Honoring S. Gordon Castigliano, M.D. cancer research at Mayo Clinic Florida (JAC).

We thank Dr. Jason Hall for editing of this manuscript and Dr. Antonio DiCristofano for helpful suggestions. We are greatly appreciative to Drs. James Fagin and Jeffrey Knauf for mutational analysis of our four ATC cell lines.

References

Panobinostat approved for multiple myeloma. Cancer discovery. 2015; 5:OF4.

Ader I, Toulas C, Dalenc F, Delmas C, Bonnet J, Cohen-Jonathan E, Gilles Favre G. RhoB controls the 24 kDa FGF-2-induced radioresistance in HeLa cells by preventing post-mitotic cell death. Oncogene. 2002; 21:5998–6006. [PubMed: 12203112]

Adnane J, Muro-Cacho C, Mathews L, Sebti SM, Munoz-Antonia T. Suppression of Rho B Expression in Invasive Carcinoma from Head and Neck Cancer Patients. Clinical cancer research : an official journal of the American Association for Cancer Research. 2002; 8:2225–2232. [PubMed: 12114424]

Agarwal B, Halmos B, Feoktistov AS, Protiva P, Ramey WG, Chen M, Pothoulakis C, Lamont JT, Holt PR. Mechanism of lovastatin-induced apoptosis in intestinal epithelial cells. Carcinogenesis. 2002; 23:521–528. [PubMed: 11895868]

Ahn J, Choi J-H, Won M, Kang C-M, Gyun M-R, Park H-M, Kim C-H, Chung K-S. The activation of p38 MAPK primarily contributes to UV-induced RhoB expression by recruiting the c-Jun and p300 to the distal CCAAT box of the RhoB promoter. Biochemical and Biophysical Research Communications. 2011; 409:211–216. [PubMed: 21565167]

Ain KB, Egorin MJ, DeSimone PA. Treatment of anaplastic thyroid carcinoma with paclitaxel: phase 2 trial using ninety-six-hour infusion. Collaborative Anaplastic Thyroid Cancer Health Intervention Trials (CATCHIT) Group. Thyroid. 2000; 10:587–594. [PubMed: 10958311]

Akiyama T, Dass CR, Choong PF. Bim-targeted cancer therapy: a link between drug action and underlying molecular changes. Mol Cancer Ther. 2009; 8:3173–3180. [PubMed: 19934277]

Allal C, Pradines A, Hamilton AD, Sebti SM, Favre G. Farnesylated RhoB prevents cell cycle arrest and actin cytoskeleton disruption caused by the geranylgeranyltransferase I inhibitor GGTI-298. Cell Cycle. 2002; 1:430–437. [PubMed: 12548020]

Altmann A, Markert A, Askoxylakis V, Schöning T, Jesenofsky R, Eisenhut M, Haberkorn U. Antitumor Effects of Proteasome Inhibition in Anaplastic Thyroid Carcinoma. Journal of Nuclear Medicine. 2012; 53:1764–1771. [PubMed: 23055533]

Bertos N, Wang A, Yang X. Class II histone deacetylases: structure, function, and regulation. Biochem Cell Biol. 2001; 79:243–252. [PubMed: 11467738]

Borbone E, Berlingieri MT, De Bellis F, Nebbioso A, Chiappetta G, Mai A, Altucci L, Fusco A. Histone deacetylase inhibitors induce thyroid cancer-specific apoptosis through proteasome-dependent inhibition of TRAIL degradation. Oncogene. 2010; 29:105–116. [PubMed: 19802013]

Boyault C, Gilquin B, Zhang Y, Rybin V, Garman E, Meyer-Klaucke W, Matthias P, Muller CW, Khochbin S. HDAC6-p97/VCP controlled polyubiquitin chain turnover. EMBO J. 2006; 25:3357–3366. [PubMed: 16810319]

Boyault C, Sadoul K, Pabion M, Khochbin S. HDAC6, at the crossroads between cytoskeleton and cell signaling by acetylation and ubiquitination. Oncogene. 2007; 26:5468–5476. [PubMed: 17694087]

Catalano MG, Poli R, Pugliese M, Fortunati N, Boccuzzi G. Valproic acid enhances tubulin acetylation and apoptotic activity of paclitaxel on anaplastic thyroid cancer cell lines. Endocrine-Related Cancer. 2007; 14:839–845. [PubMed: 17914112]

Chakraborty AR, Robey RW, Luchenko VL, Zhan Z, Piekarz RL, Gillet JP, Kossenkov AV, Wilkerson J, Showe LC, Gottesman MM, et al. MAPK pathway activation leads to Bim loss and histone deacetylase inhibitor resistance: rationale to combine romidepsin with an MEK inhibitor. Blood. 2013; 121:4115–4125. [PubMed: 23532732]

Chan D, Zheng Y, Tyner J, Chng W, Chien W, Gery S, Leong G, Braunstein G, Koeffler HP. Belinostat and panobinostat (HDACI): in vitro and in vivo studies in thyroid cancer. Journal of Cancer Research and Clinical Oncology. 2013:1–8.

Chen Y-X, Li Z-B, Diao F, Cao D-M, Fu C-C, Lu J. Up-regulation of RhoB by glucocorticoids and its effects on the cell proliferation and NF-[kappa]B transcriptional activity. The Journal of Steroid Biochemistry and Molecular Biology. 2006; 101:179–187. [PubMed: 17046241]

Chou TC, Talalay P. Quantitative analysis of dose-effect relationships: the combined effects of multiple drugs or enzyme inhibitors. Adv Enzyme Regul. 1984; 22:27–55. [PubMed: 6382953]

Collins NL, Reginato MJ, Paulus JK, Sgroi DC, LaBaer J, Brugge JS. G1/S Cell Cycle Arrest Provides Anoikis Resistance through Erk-Mediated Bim Suppression. Molecular and Cellular Biology. 2005; 25:5282–5291. [PubMed: 15923641]

Copland JA, Marlow LA, Kurakata S, Fujiwara K, Wong AK, Kreinest PA, Williams SF, Haugen BR, Klopper JP, Smallridge RC. Novel high-affinity PPARgamma agonist alone and in combination with paclitaxel inhibits human anaplastic thyroid carcinoma tumor growth via p21WAF1/CIP1. Oncogene. 2006; 25:2304–2317. [PubMed: 16331265]

Delarue FL, Adnane J, Joshi B, Blaskovich MA, Wang DA, Hawker J, Bizouarn F, Ohkanda J, Zhu K, Hamilton AD, et al. Farnesyltransferase and geranylgeranyltransferase I inhibitors upregulate RhoB expression by HDAC1 dissociation, HAT association and histone acetylation of the RhoB promoter. Oncogene. 2007; 26:633–640. [PubMed: 16909123]

Du W, Prendergast GC. Geranylgeranylated RhoB mediates suppression of human tumor cell growth by farnesyltransferase inhibitors. Cancer Res. 1999; 59:5492–5496. [PubMed: 10554025]

Fritz G, Kaina B. Transcriptional activation of the small GTPase gene rhoB by genotoxic stress is regulated via a CCAAT element. Nucl Acids Res. 2001; 29:792–798. [PubMed: 11160903]

Furumai R, Matsuyama A, Kobashi N, Lee KH, Nishiyama M, Nakajima H, Tanaka A, Komatsu Y, Nishino N, Yoshida M, et al. FK228 (depsipeptide) as a natural prodrug that inhibits class I histone deacetylases. Cancer Res. 2002; 62:4916–4921. [PubMed: 12208741]

Gao L, Cueto MA, Asselbergs F, Atadja P. Cloning and Functional Characterization of HDAC11, a Novel Member of the Human Histone Deacetylase Family. Journal of Biological Chemistry. 2002; 277:25748–25755. [PubMed: 11948178]

Ishida H, Zhang X, Erickson K, Ray P. Botulinum Toxin Type A Targets RhoB to Inhibit Lysophosphatidic Acid-Stimulated Actin Reorganization and Acetylcholine Release in Nerve Growth Factor-Treated PC12 Cells. J Pharmacol Exp Ther. 2004; 310:881–889. [PubMed: 15140914]

Jiang K, Delarue FL, Sebti SM. EGFR, ErbB2 and Ras but not Src suppress RhoB expression while ectopic expression of RhoB antagonizes oncogene-mediated transformation. Oncogene. 2003; 23:1136–1145. [PubMed: 14647415]

Jiang K, Sun J, Cheng J, JYD, Wei S, Sebti S. Akt Mediates Ras Downregulation of RhoB, a Suppressor of Transformation, Invasion, and Metastasis. Mol Cell Biol. 2004; 24:5565–5576. [PubMed: 15169915]

Kaliszczak M, Trousil S, Aberg O, Perumal M, Nguyen QD, Aboagye EO. A novel small molecule hydroxamate preferentially inhibits HDAC6 activity and tumour growth. Br J Cancer. 2013; 108:342–350. [PubMed: 23322205]

Khan N, Jeffers M, Kumar S, Hackett C, Boldog F, Khramtsov N, Qian X, Mills E, Berghs SC, Carey N, et al. Determination of the class and isoform selectivity of small-molecule histone deacetylase inhibitors. Biochem J. 2008; 409:581–589. [PubMed: 17868033]

Kim B-K, Im J-Y, Han G, Lee W-J, Won K-J, Chung K-S, Lee K, Ban HS, Song K, Won M. p300 cooperates with c-Jun and PARP-1 at the p300 binding site to activate RhoB transcription in NSC126188-mediated apoptosis. Biochimica et Biophysica Acta (BBA) - Gene Regulatory Mechanisms. 2014; 1839:364–373. [PubMed: 24636898]

Lee HZ, Kwitkowski VE, Del Valle PL, Ricci MS, Saber H, Habtemariam BA, Bullock J, Bloomquist E, Li Shen Y, Chen XH, et al. FDA Approval: Belinostat for the Treatment of Patients with Relapsed or Refractory Peripheral T-cell Lymphoma. Clinical cancer research : an official journal of the American Association for Cancer Research. 2015

Li Y, Shin D, Kwon SH. Histone deacetylase 6 plays a role as a distinct regulator of diverse cellular processes. FEBS Journal. 2013; 280:775–793. [PubMed: 23181831]

Li Y, Zhang X, Polakiewicz RD, Yao T-P, Comb MJ. HDAC6 Is Required for Epidermal Growth Factor-induced β-Catenin Nuclear Localization. Journal of Biological Chemistry. 2008; 283:12686–12690. [PubMed: 18356165]

Mai A, Massa S, Pezzi R, Simeoni S, Rotili D, Nebbioso A, Scognamiglio A, Altucci L, Loidl P, Brosch G. Class II (IIa)-selective histone deacetylase inhibitors. 1. Synthesis and biological evaluation of novel (aryloxopropenyl)pyrrolyl hydroxyamides. J Med Chem. 2005; 48:3344–3353. [PubMed: 15857140]

Marlow LA, D'Innocenzi J, Zhang Y, Rohl SD, Cooper SJ, Sebo T, Grant C, McIver B, Kasperbauer JL, Wadsworth JT, et al. Detailed molecular fingerprinting of four new anaplastic thyroid carcinoma cell lines and their use for verification of RhoB as a molecular therapeutic target. J Clin Endocrinol Metab. 2010; 95:5338–5347. [PubMed: 20810568]

Marlow LA, Reynolds LA, Cleland AS, Cooper SJ, Gumz ML, Kurakata S, Fujiwara K, Zhang Y, Sebo T, Grant C, et al. Reactivation of suppressed RhoB is a critical step for the inhibition of anaplastic thyroid cancer growth. Cancer Res. 2009; 69:1536–1544. [PubMed: 19208833]

Mazieres J, Antonia T, Daste G, Muro-Cacho C, Berchery D, Tillement V, Pradines A, Sebti S, Favre G. Loss of RhoB Expression in Human Lung Cancer Progression. Clinical cancer research : an official journal of the American Association for Cancer Research. 2004; 10:2742–2750. [PubMed: 15102679]

Mazieres J, Tillement V, Allal C, Clanet C, Bobin L, Chen Z, Sebti SM, Favre G, Pradines A. Geranylgeranylated, but not farnesylated, RhoB suppresses Ras transformation of NIH-3T3 cells. Experimental Cell Research. 2005; 304:354–364. [PubMed: 15748883]

Mitsiades CS, Poulaki V, McMullan C, Negri J, Fanourakis G, Goudopoulou A, Richon VM, Marks PA, Mitsiades N. Novel histone deacetylase inhibitors in the treatment of thyroid cancer. Clinical cancer research : an official journal of the American Association for Cancer Research. 2005; 11:3958–3965. [PubMed: 15897598]

Nebbioso A, Manzo F, Miceli M, Conte M, Manente L, Baldi A, De Luca A, Rotili D, Valente S, Mai A, et al. Selective class II HDAC inhibitors impair myogenesis by modulating the stability and activity of HDAC-MEF2 complexes. EMBO reports. 2009; 10:776–782. [PubMed: 19498465]

New M, Olzscha H, La Thangue NB. HDAC inhibitor-based therapies: Can we interpret the code? Molecular Oncology. 2012; 6:637–656. [PubMed: 23141799]

Noguchi H, Yamashita H, Murakami T, Hirai K, Noguchi Y, Maruta J, Yokoi T, Noguchi S. Successful Treatment of Anaplastic Thyroid Carcinoma with a Combination of Oral Valproic Acid, Chemotherapy, Radiation and Surgery. Endocrine Journal. 2009; 56:245–249. [PubMed: 19088401]

Prendergast G. Farnesyltransferase inhibitors define a role for RhoB in controlling neoplastic pathophysiology. Histol Histopathol. 2001a; 16:269–275. [PubMed: 11193202]

Prendergast GC. ACTIN' UP: RHOB IN CANCER AND APOPTOSIS. Nature Reviews Cancer. 2001b; 1:162–168.

Prince HM, Bishton MJ, Harrison SJ. Clinical studies of histone deacetylase inhibitors. Clinical cancer research : an official journal of the American Association for Cancer Research. 2009; 15:3958–3969. [PubMed: 19509172]

Ramesh S, Wildey GM, Howe PH. Transforming growth factor β (TGFβ)-induced apoptosis: The rise and fall of Bim. Cell Cycle. 2009; 8:11–17. [PubMed: 19106608]

Sambucetti LC, Fischer DD, Zabludoff S, Kwon PO, Chamberlin H, Trogani N, Xu H, Cohen D. Histone deacetylase inhibition selectively alters the activity and expression of cell cycle proteins leading to specific chromatin acetylation and antiproliferative effects. J Biol Chem. 1999; 274:34940–34947. [PubMed: 10574969]

Schmittgen TD, Livak KJ. Analyzing real-time PCR data by the comparative C(T) method. Nat Protoc. 2008; 3:1101–1108. [PubMed: 18546601]

Smallridge RC, Copland JA, Brose MS, Wadsworth JT, Houvras Y, Menefee ME, Bible KC, Shah MH, Gramza AW, Klopper JP, et al. Efatutazone, an Oral PPAR-γ Agonist, in Combination with Paclitaxel in Anaplastic Thyroid Cancer: Results of a Multicenter Phase 1 Trial. Journal of Clinical Endocrinology & Metabolism. 2013; 98:2392–2400. [PubMed: 23589525]

Smallridge RC, Marlow LA, Copland JA. Anaplastic thyroid cancer: molecular pathogenesis and emerging therapies. Endocr Relat Cancer. 2009; 16:17–44. [PubMed: 18987168]

Srougi MC, Burridge K. The nuclear guanine nucleotide exchange factors Ect2 and Net1 regulate RhoB-mediated cell death after DNA damage. PLoS ONE. 2011; 6:e17108. [PubMed: 21373644]

Vaziri H, Dessain SK, Eaton EN, Imai S-I, Frye RA, Pandita TK, Guarente L, Weinberg RA. hSIR2SIRT1 Functions as an NAD-Dependent p53 Deacetylase. Cell. 2001; 107:149–159. [PubMed: 11672523]

Vishnu P, Colon-Otero G, Kennedy GT, Marlow LA, Kennedy WP, Wu KJ, Santoso JT, Copland JA. RhoB mediates antitumor synergy of combined ixabepilone and sunitinib in human ovarian serous cancer. Gynecol Oncol. 2012; 124:589–597. [PubMed: 22115851]

Wang S, Yan-Neale Y, Fischer D, Zeremski M, Cai R, Zhu J, Asselbergs F, Hampton G, Cohen D. Histone deacetylase 1 represses the small GTPase RhoB expression in human nonsmall lung carcinoma cell line. Oncogene. 2003; 22:6204–6213. [PubMed: 13679859]

Wang S, Yan-Neale Y, Zeremski M, Cohen D. Transcription regulation by histone deacetylases. Novartis Found Symp. 2004; 259:238–245. [PubMed: 15171258]

Zhao Y, Tan J, Zhuang L, Jiang X, Liu ET, Yu Q. Inhibitors of histone deacetylases target the Rb-E2F1 pathway for apoptosis induction through activation of proapoptotic protein Bim. Proceedings of the National Academy of Sciences of the United States of America. 2005; 102:16090–16095. [PubMed: 16243973]

Zhou X, Marks PA, Rifkind RA, Richon VM. Cloning and characterization of a histone deacetylase, HDAC9. Proceedings of the National Academy of Sciences. 2001; 98:10572–10577.

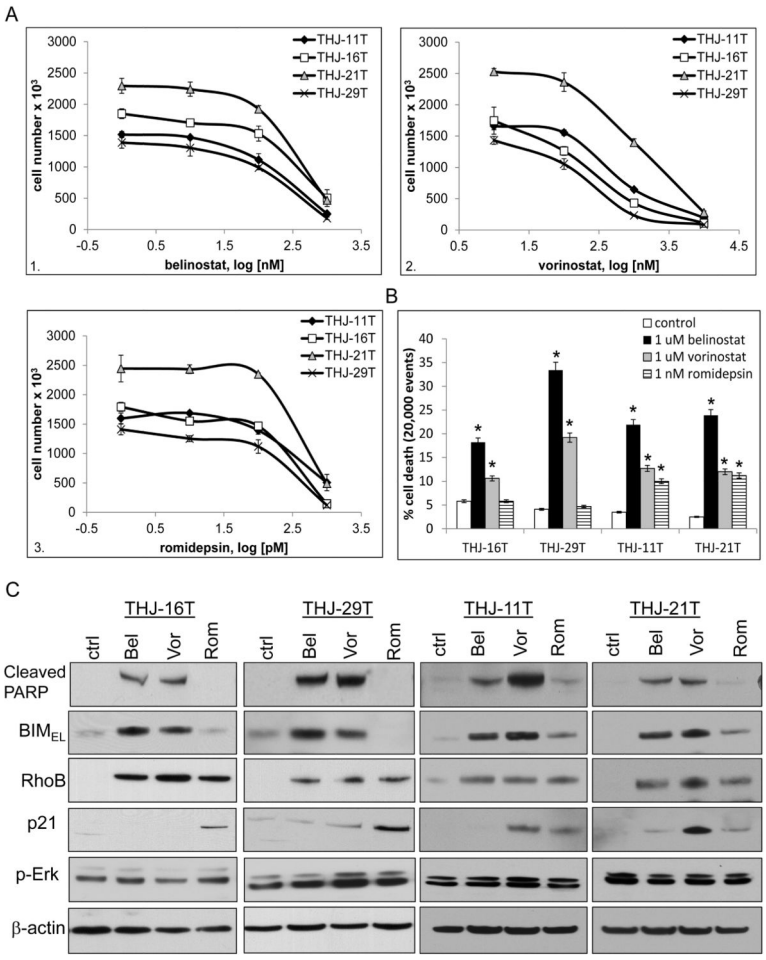

Figure 1. Comparison of class I and I/II HDAC inhibitors in ATC cell lines

For dose out curves, ATC cells were plated in triplicate in 12-well culture plates at 2×10^4 cells/well and treated for 72 h. Data was plotted on log scale for drug concentrations vs. cell number ± S.D. **A**. The class II(I) hydroxamate inhibitors: belinostat (PXD101) yielded IC_{50} of 400 nM for both THJ-16T and THJ-21T and 250 nM for both THJ-11T and THJ-29T (panel 1) while vorinostat (SAHA) yielded IC_{50} of 250 nM for both THJ-16T and THJ-29T and 450 to 500 nM for THJ-11T and THJ-21T (panel 2). The cyclic peptide class I inhibitor: romidepsin (FK-228) yielded IC_{50} of 0.4 nM for all 4 cell lines (panel 3). **B**. For cell death, cells were grown to ~ 50% confluence and treated with either 1 μM belinostat (Bel), 1 μM vorinostat (Vor) or 1 nM romidepsin (Rom) for 72 h prior to flow cytometry with propidium iodide. Data is plotted as average percent cell death within 20,000 events ± S.D. *indicated $p<0.05$ was considered statistically significant when compared to DMSO control. **C**. For western blots, cells were treated for 24 h and analyzed by western blot for p-Erk, RhoB and p21. BIM_{EL} and cleaved PARP were indicators of apoptosis and β-actin was used as a loading control.

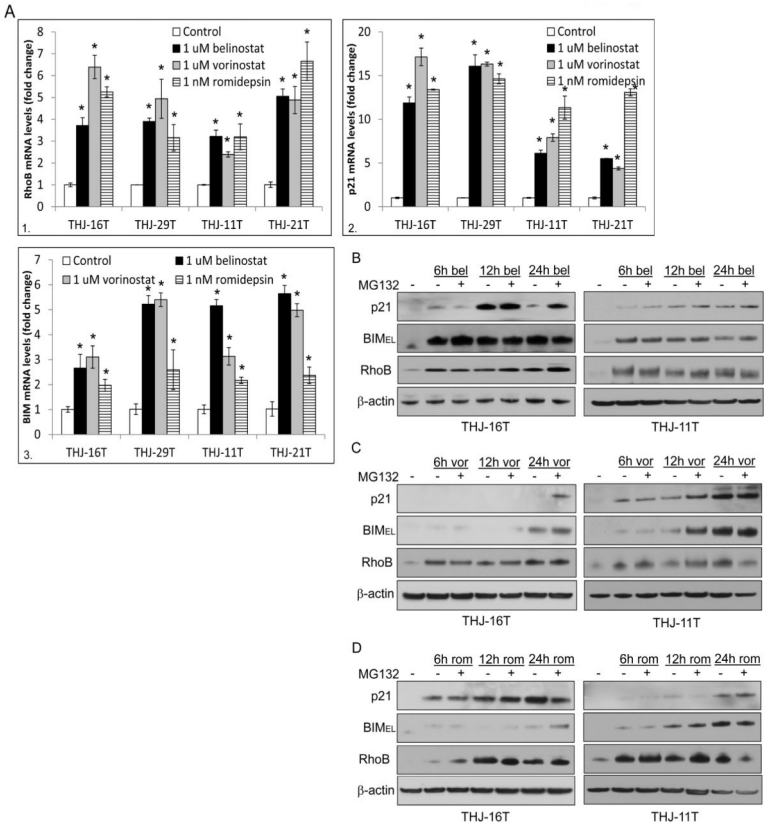

Figure 2. HDAC inhibitors have different p21 / BIM_{EL} mRNA and protein expression

A. For verification of transcriptional activation of RhoB and p21 (Figure s1), QPCR was done in cells treated for 24 h with HDACi (panel 1–2). QPCR was also performed for BCL2L11 (BIM) mRNA levels and elevated in all HDACi treated cells (panel 3). Data was plotted as fold change ± S.D. *indicated $p<0.05$ was considered statistically significant when compared to DMSO control. **B**. Western blot analysis of THJ-16T and THJ-11T cells treated with belinostat alone or in combination with 1 nM MG132 (a proteasome inhibitor) at the indicated time points was done for monitoring protein stability. **C**. Western blot analysis was performed for vorinostat alone or in combination with 1 nM MG132. **D**. Western blot analysis was performed for romidepsin alone or in combination with 1 nM MG132.

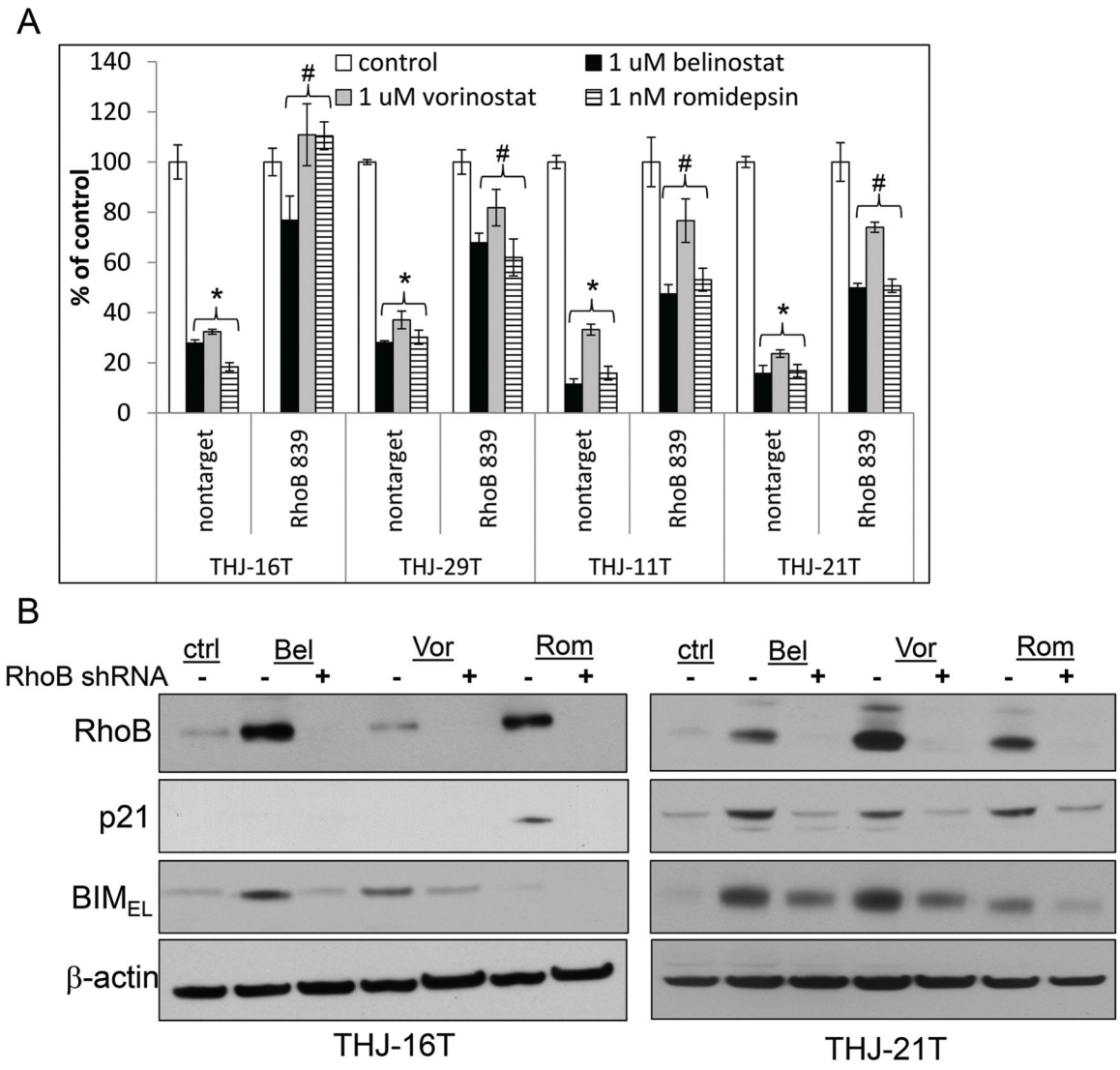

Figure 3. Both p21 and BIM are RhoB dependent

A. Nontarget and RhoB 839 shRNA silenced cells were plated in triplicate in 12-well culture plates at 2 × 10^4 cells/well and treated for 72 h with 1 μM belinostat, 1 μM vorinostat and 1 nM romidepsin. Data was plotted as cell number ± S.D. * indicated $p<0.05$ was considered statistically significant when compared to untreated control. # indicated $p<0.05$ was considered statistically significant when compared to applicable nontarget treatment. **B**. Western blot analysis of nontarget and RhoB 839 shRNA cells treated for 24 h showed that BIM_{EL} and p21 were blocked when RhoB was silenced. β-actin was used as a loading control.

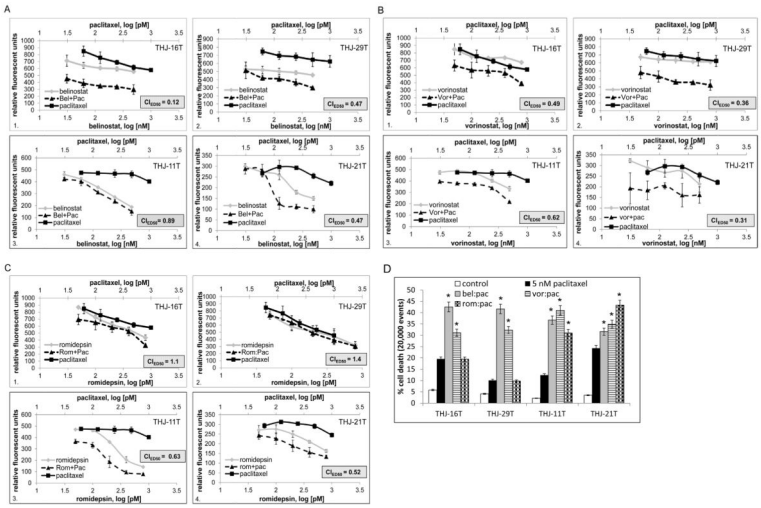

Figure 4. Synergy of HDAC inhibitors and paclitaxel were dependent upon presence of BIM expression

ATC cells were plated at 2,500 cells/well and treated for 72 h prior to CyQUANT analysis. Experiments were carried out using HDAC inhibitors, paclitaxel and a fixed ratio combination of both at a variety of different doses as indicated. **A**. Belinostat in combination with paclitaxel demonstrated synergy as indicated by the left shift and CI_{ED50} value < 1.0. ED50 is effective dose at 50% **B**. Vorinostat also had synergy when combined with paclitaxel as indicated by CI_{ED50} value < 1.0. **C**. Romidepsin did not have synergy (CI_{ED50} value > 1.0) when combined with paclitaxel in THJ-16T and THJ-29T, which did not have BIM_{EL} expression (panels 1–2). On the other hand, romidepsin did have synergy with paclitaxel in THJ-11T and THJ-21T, which do have BIM_{EL} expression (panels 3–4) and have KRAS and BRAF mutations, respectively. **D**. Cell death analysis after 72 hours with combinatorial therapy demonstrated enhanced cell death with the Class II HDAC inhibitors, but not with romidepsin when compared to paclitaxel alone in THJ-16T and THJ-29T. Cell death was observed with all HDACi for both THJ-11T and THJ-21T. Data is plotted as average percent cell death within 20,000 events ± S.D. *indicated $p<0.05$ was considered statistically significant when compared to DMSO control.

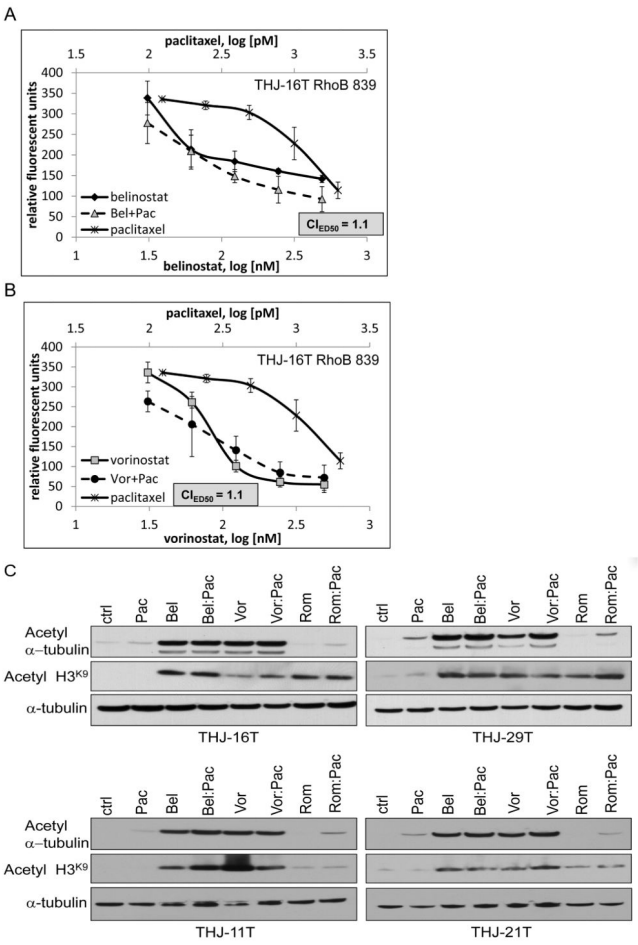

Figure 5. Combinatorial synergy is dependent upon RhoB and not acetylated α-tubulin

A. Using THJ-16T, belinostat in combination with paclitaxel lost its synergy when RhoB was silenced as indicated by CI_{ED50} value > 1.0. **B.** Vorinostat in combination with paclitaxel also lost its synergy when RhoB was silenced as indicated by CI_{ED50} value > 1.0. **B.** ATC cells were treated with HDACi and paclitaxel alone or in combination for 24 h to verify HDAC inhibitor and paclitaxel activities via increased expression of acetyl a-tubulin when treated alone or in combination. α-tubulin was used as a loading control.

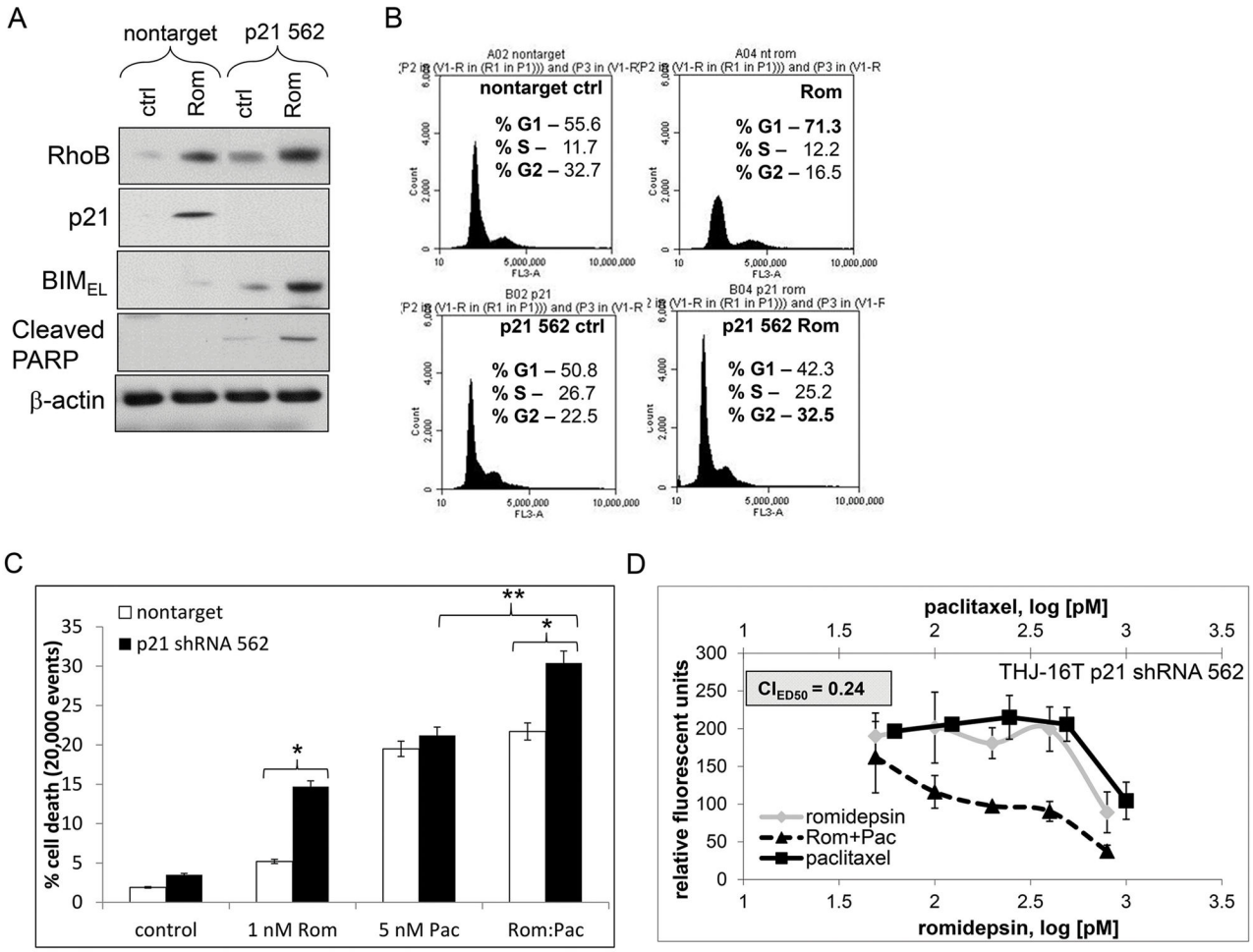

Figure 6. Silencing p21 in the presence of romidepsin shifts RhoB to the BIM pathway

A. Western blot analysis of the p21 562 construct in THJ-16T cells demonstrated that RhoB remained induced upon romidepsin treatment while BIM_{EL} and PARP cleavage was induced when p21 was silenced. β-actin was used as a loading control. **B**. Cell cycle analysis after 72 h with romidepsin treatment was done to examine shifting in the G1 phase and G2 phase reversal. **C**. Cell death analysis with 72 h treatment showed that romidepsin does not induce cell death unless p21 is silenced. * indicated $p<0.05$ was considered statistically significant when compared to applicable nontarget ** indicated $p<0.05$ was considered statistically significant when compared to paclitaxel alone. **D**. When p21 was silenced, romidepsin and paclitaxel showed combinatorial synergy in both cell death and cell growth inhibition as indicated by CI_{ED50} value < 1.0.

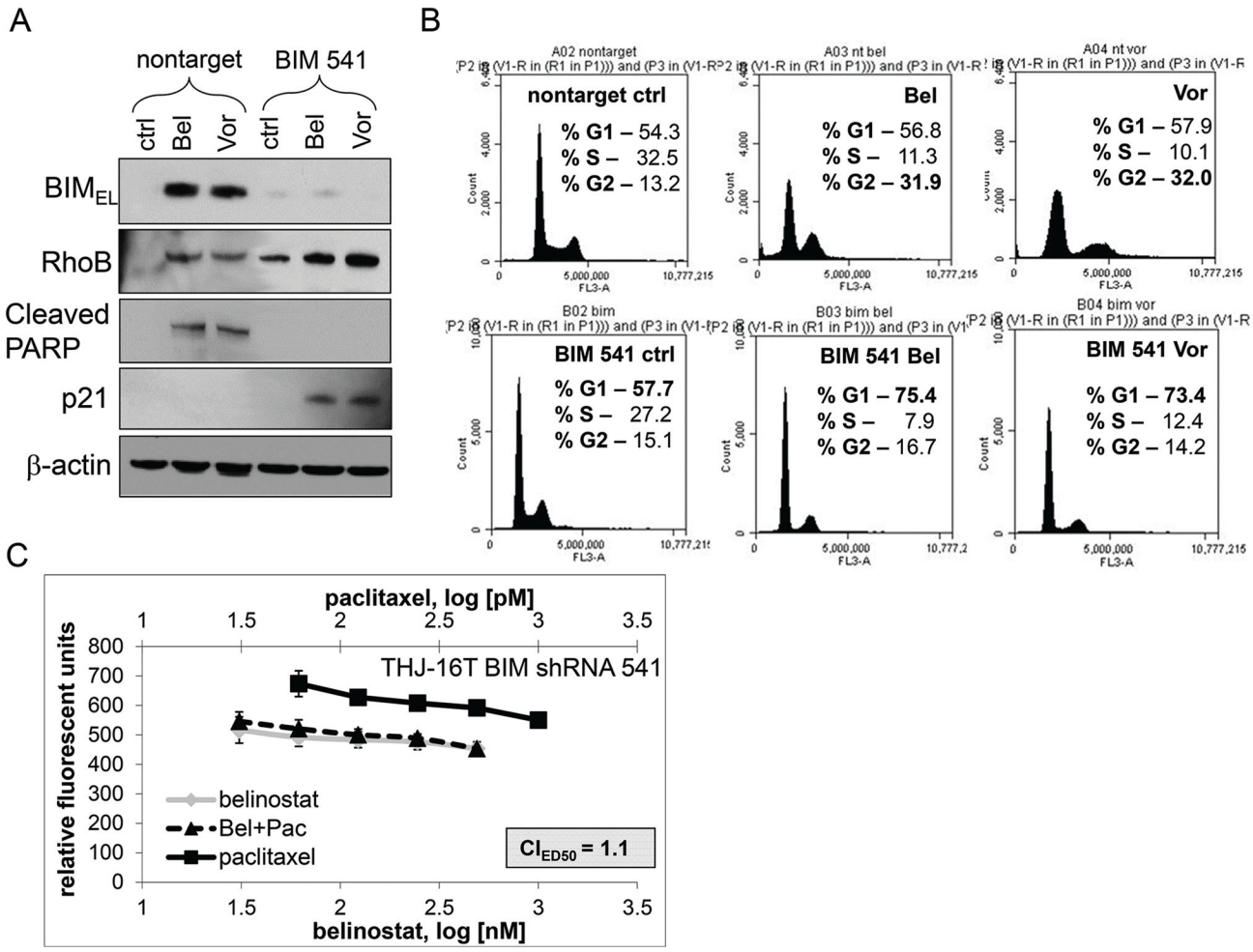

Figure 7. Silencing BIM in the presence of belinostat and vorinostat shifts RhoB to the p21 pathway

A. Western blot analysis using the BIM 541 construct in THJ-16T cells was examined for effects upon downstream targets. PARP cleavage was lost when BIM was silenced and p21 expression was induced. β-actin was used as a loading control. **B**. Cell cycle analysis after 24 h treatment with belinostat and vorinostat treatment was done to examine shifting in the G2 phase and G1 phase reversal. **C**. Combinatorial synergy was lost with belinostat and paclitaxel when BIM_{EL} was silenced.

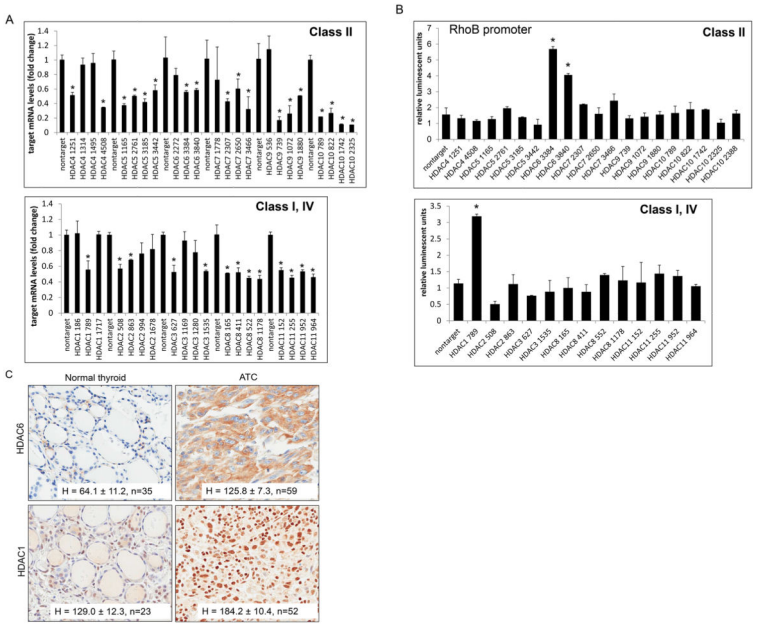

Figure 8. Identification of HDAC1 and HDAC6 as repressors of RhoB

A. THJ-16T cells were transiently transfected with MISSION shRNA pLKO.1 constructs: nontarget, HDAC1 (clones NM_004964.2), HDAC2 (clones NM_001527.1), HDAC3 (clones NM_003883.2), HDAC4 (clones NM_006037.2), HDAC5 (clones NM_005474.3), HDAC6 (clones NM_006044.2), HDAC7 (clones NM_015401.1), HDAC8 (clones NM_018486.1), HDAC9 (clones NM_014707.1), HDAC10 (clones NM_032019.4), and HDAC11 (clones NM_024827.1). The construct clone numbers are as indicated. QPCR was performed for each set of HDACs in order to examine level of silencing. **B**. Luciferase RhoB reporter assay for screening transcription regulation by HDACs from class I, II and IV. THJ-16T cells were transiently transfected with renilla, RhoB-luc and verified MISSION shRNA pLKO.1 constructs as indicated. Luciferase data was normalized for transfection efficiency based upon renilla activity levels and reported as relative luminescent units ± S.D. Comparisons were analyzed by two-tailed paired Student's *t*-test. *indicated, $p < 0.05$ was considered statistically significant as compared to nontarget control. **C**. IHC of patient normal and ATC tissue for HDAC1 and HDAC6 showed strong staining for both HDACs in tumor tissue as indicated by H score ± S.D. Sample size (n) was as indicated.

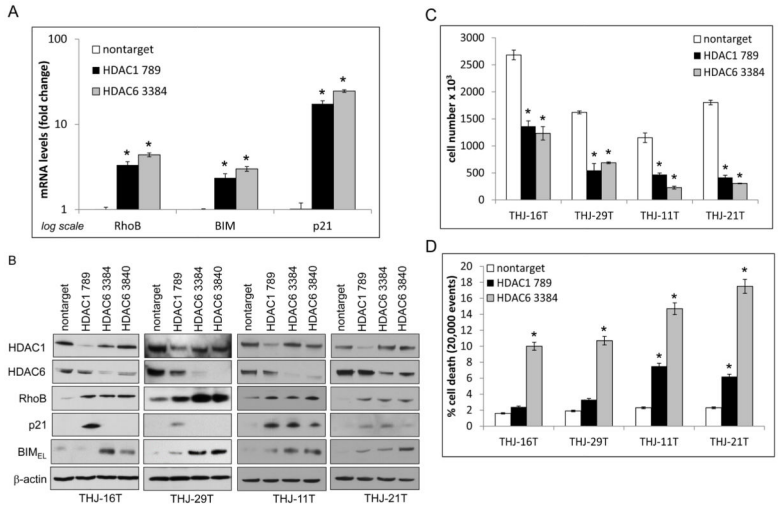

Figure 9. Downstream effects of HDAC1 and HDAC6

A. QPCR of RhoB, p21 and BIM in HDAC1 and HDAC6 silenced THJ-16T cells show that all 3 mRNAs are upregulated. **B.** Western blot analysis of nontarget, HDAC1 789, HDAC6 3384 and HDAC6 3840 shRNA clones were examined for differential downstream targets effects. β-actin was used as a loading control. **C.** Nontarget and HDAC shRNA cells were selected for 24 h and then plated in triplicate in 12-well culture plates at 2×10^4 cells/well for 72 h. Data was plotted as cell number ± S.D. * indicated $p<0.05$ was considered statistically significant when compared to nontarget control. **D**. After 36 h selection, cells were plated for cell death analysis and incubated for 72 h prior to flow cytometry with propidium iodide.

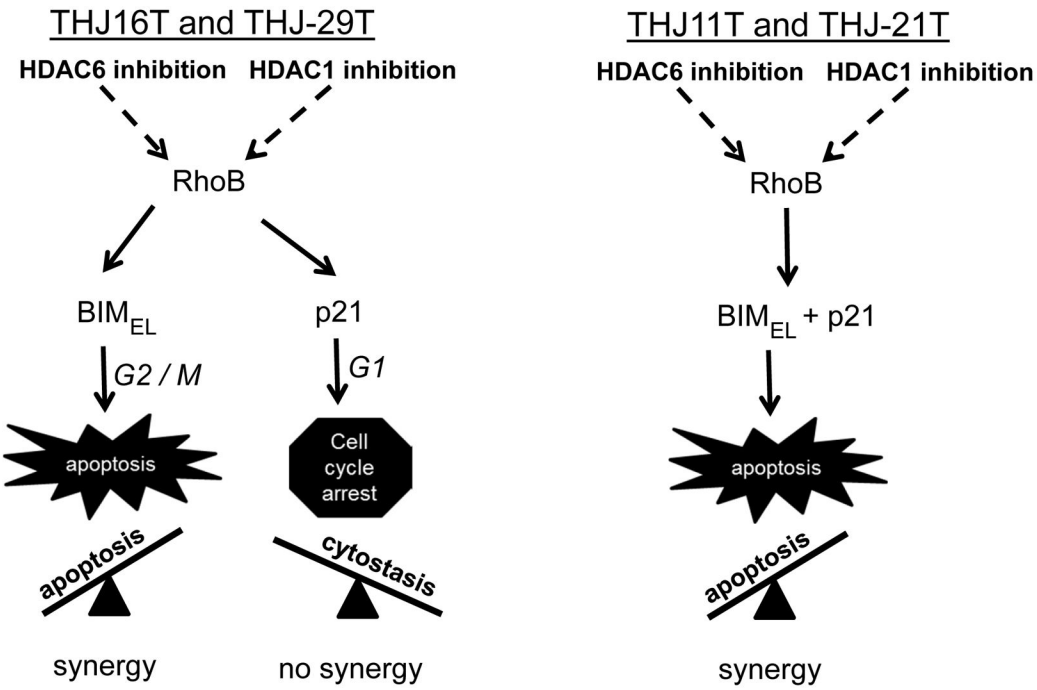

Figure 10. Divergent RhoB pathways

RhoB expression was regulated by both HDAC1 and HDAC6 and inhibition of these HDACs in ATC led to the dominant pathway downstream of RhoB. If BIM_{EL} was induced by RhoB, then it led to apoptosis/cell death and combinatorial synergy. If p21 was exclusively induced by RhoB, then it led to cytostasis and no combinatorial synergy. These pathways acted as a seesaw and the dominant pathway determined the fate of the cell.